# Preparing carbon-black-coated magnetite nanoparticles: fabrication, characterization, and heterogeneous persulfate oxidation of methylene blue

## Cheng-Di Dong, Chiu-Wen Chen, Chang-Mao Hung*

*Department of Marine Environmental Engineering, National Kaohsiung Marine University, 142 Haijhuan Road, Nanzih District, Kaohsiung City 81157, Taiwan, Tel. +886-7-3617141 Ext. 3777; Fax: +886-7-3650548; email: hungcm1031@gmail.com (C.-M. Hung); Tel. +886-7-3617141 Ext. 3762; email: cddong@mail.nkmu.edu.tw (C.-D. Dong); Tel. +886-7-3617141 Ext. 3761; email: cwchen@mail.nkmu.edu.tw (C.-W. Chen)*

### ABSTRACT

The aim of this study was persulfate (PS) oxidation of methylene blue (MB) using iron oxide–carbon black ($Fe_3O_4$–CB) as heterogeneous catalyst in aqueous solution. The oxidation reaction was optimized based on enlisted factors: the initial pH, PS concentration, and $Fe_3O_4$–CB amount. The degradation kinetics and reactivity of the catalyst were also investigated. The decolorization rate of MB showed strong pH dependence. The degradation process followed the pseudo-first-order kinetic model. The catalyst were characterized by using X-ray diffraction (XRD), a superconducting quantum interference device magnetometry, fluorescence spectroscopy, ultraviolet-visible spectroscopy, cyclic voltammetry (CV), Brunauer–Emmett–Teller analysis, and environmental scanning electron microscopy (ESEM). XRD analysis indicated the existence of $Fe_3O_4$ on the composite surface. The magnetic properties of $Fe_3O_4$–CB showed great saturation magnetization (Ms). The CV reversible redox ability explained the high activity of the $Fe_3O_4$–CB composite, and the oxidation current density on the $Fe_3O_4$–CB composite increased with the scan rate. ESEM–EDS measurements revealed the presence of $Fe_3O_4$ crystal nanoparticles on the CB-supported surface and resulting in higher surface area up to 1,965 $m^2\,g^{-1}$. These spherical crystal phases dispersed in the CB matrix with sizes of 50–100 nm may explain the high activity of the composite in heterogeneous $SO_4^{-\bullet}$-based advanced oxidation process reaction, which is also responsible for the strong metal-support interaction.

*Keywords:* Iron oxide–carbon black composites; Persulfate oxidation; Methylene blue; Cyclic voltammetry

## 1. Introduction

Much attention has been paid to organic dyes due to their wide recognition as one of the most ubiquitous pollutants exposure to aquatic organisms and natural environments [1–11]. The dyes usually with complex aromatic structure emitted in different process from leather, pharmaceutical, textile and so on industries, which has mutagenic and carcinogenic properties [12–14]. Therefore, extensive study has been carried out to develop removing industrial dyes from waste streams and controlled dye effluents. In the past dec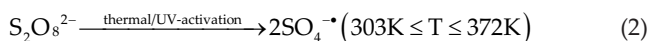ades, variety of techniques had been developed, for example, biodegradation, filtration, coagulation, ozonation, UV-light irradiation, catalytic oxidation, adsorption, and so on, for the elimination of dye from effluent water [15]. However, the above technologies either result in phase transformation or yield sludge as a toxic by-product, which is an additional environmental contaminant, or require further complete detoxification of the pollutant to conform the stringent discharge regulations.

To overcome the limitations of conventional process, highly reactive sulfate anion radical ($SO_4^{-\bullet}$) has been demonstrated as powerful oxidizing species for degradation of dye effluents [16–19]. Generally, persulfate (PS) can be chemically activated by transition metal ions ($M^{n+}$), thermally or
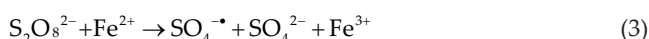
---

\* Corresponding author.

ultraviolet light activated to generate strong oxidizing species of $SO_4^{-\bullet}$ [20], and have been utilized for such processes.

$$S_2O_8^{2-} + M^{n+} \xrightarrow{\text{chemical-activation}} SO_4^{-\bullet} + SO_4^{2-} + M^{(n+1)+} \qquad (1)$$

$$S_2O_8^{2-} \xrightarrow{\text{thermal/UV-activation}} 2SO_4^{-\bullet} \left(303K \leq T \leq 372K\right) \qquad (2)$$
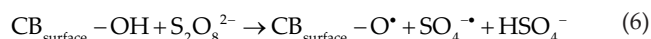
However, this crucial heterogeneous catalytic process has attracted considerable attention in materials chemistry, and the effectiveness through electron transfer process has been improved using high-performance Fe(II), which generates $SO_4^{-\bullet}$ and hydroxyl free radicals ($\bullet$OH) in a manner similar to that of Fenton's reaction.

$$S_2O_8^{2-} + Fe^{2+} \rightarrow SO_4^{-\bullet} + SO_4^{2-} + Fe^{3+} \qquad (3)$$

$$SO_4^{-\bullet} + H_2O \rightarrow HO\bullet + HSO_4^- \qquad (4)$$

Therefore, the use of a suitable metal oxide in the PS approach might yield an effective reactive species that can rapidly removal contaminants. Because of their engineering effectiveness, $SO_4^{-\bullet}$-based advanced oxidation process (AOPs) selectively produce carbon dioxide and oxidize small molecules through aqueous-phase oxidation. Generally, various types of adsorbent and catalyst have been widely enhanced in the treatment of dye-contaminated wastewater. Asfaram et al. applied the novel composite Mn–$Fe_3O_4$–NPs–AC adsorbent with ultrasonic power for removal methylene blue (MB) reached 99.54% after 3 min, while their equilibrium data can be represented by Langmuir isotherms and a pseudo-second-order kinetic model for fitting experimental data indicates economic and profitable adsorption capacity (229.4 mg $g^{-1}$) that confirms for wastewater treatments [6]. The potential of $Fe_3O_4$ catalyst activated by peroxydisulfate in an electro–$Fe_3O_4$–peroxydisulfate process for the treatment of azo dye acid orange 7 (AO7) polluted wastewater was investigated [12]. Results showed that the $Fe_3O_4$ particles were stable and reusable. The enhanced AO7 degradation by zero-valent iron catalysts was investigated [13]. Results showed that the PS activation through ultrasonic irradiation could greatly enhance the AO7 degradation conversion of the catalyst. Zhu et al. reported that the removal capabilities of core-shell Fe–$Fe_2O_3$ nanostructure (FN) materials for methyl orange in aqueous solution [21]. Their results showed that the decolorization of methyl orange was due to FN–$Na_2S_2O_8$ process degradation and 90% decolorization was achieved after 10 min of reaction. Nguyen et al. studied of the oxidation efficiencies of the $Fe_2MnO_4$ catalysts prepared using activated carbon (AC) as a supporting material on the degradation of methyl orange at pH 3.0 revealed that treating (AC) with $HNO_3$ can functionalize the carbon surface through the formation of carboxyl groups [22]. Yan et al. observed that a complete removal of sulfamonomethoxine was achieved within 15 min when 2.4 mmol $L^{-1}$ $Fe_3O_4$ magnetic nanoparticles (NPs) and 1.2 mmol $L^{-1}$ PS were used [23]. Additionally, the efficiency of $Fe^{2+}$/PS reagent in removing dye waste was further supported in a study using azo dye orange G (OG) as the targeted pollutant [24]. In this study, optimization of degradation of OG under $Fe^{2+}$/PS technique in the temperature range 293–313 K

at pH 3.5 in an aqueous stream was investigated. It was observed that the degradation of OG increased with both $Fe^{2+}$ and PS doses. The applicability of PS oxidation in the presence of suspended granular activated carbon (GAC) for a novel treatment of AO7 wastewater was attempted [25]. It observed high efficiency of decolorizing of AO7 was obtained by a synergistic effect in a GAC/PS combined system. The results also implied the potential of PS reactivity to degrade organic contaminants.

The adsorption of contaminants onto carbon black (CB) can be regarded as a pre-concentration step prior to subsequent treatments [26–32]. The use of functional groups including carboxylic groups (–$COOH_2^+$), phenolic (–$OH_2^+$), and chromenic group [27], which enhances dyes adsorption through electrostatic attraction as an activator for mediating electron transfer and reactions on CB surfaces is proposed as follows:

$$CB_{surface} - OOH + S_2O_8^{2-} \rightarrow CB_{surface} - OO^\bullet + SO_4^{-\bullet} + HSO_4^- \quad (5)$$

$$CB_{surface} - OH + S_2O_8^{2-} \rightarrow CB_{surface} - O^\bullet + SO_4^{-\bullet} + HSO_4^- \quad (6)$$

In previous works, the authors studied the environmental applications of magnetite ($Fe_3O_4$), such as the degradation of organic compounds was achieved in dye-contaminated wastewaters [33–35]. In this work, composites consisting of $Fe_3O_4$ and CB were synthesized via depositing $Fe_3O_4$ on CB by co-precipitation method, easily separable and recyclable catalyst for the degradation of MB, a brightly colored cationic thiazine dye, as a model contaminant in $SO_4^{-\bullet}$-based AOPs.

## 2. Materials and methods

### 2.1. Chemicals and reagents

Ferric chloride hexahydrate ($FeCl_3 \bullet 6H_2O$) was obtained from Showa Chemical Co., Ltd. (Japan); ferrous chloride tetrahydrate ($FeCl_2 \bullet 4H_2O$) was purchased from Alfa Aesar, Johnson Matthey Company (USA); ammonium hydroxide ($NH_4OH$, 28%) was obtained from Fluka Chemical Co., Ltd (Germany); hydroxypropyl cellulose was purchased from Sigma-Aldrich (USA). Degussa FW200 CB was obtained from Uni-Ward Co. Ltd (Taiwan). MB was purchased from Kojima Chemicals Co., Ltd. (Japan). Sodium PS ($Na_2S_2O_8$, 98%) was purchased from Showa Chemical Industry Co. (Japan). All reagents used in the preparation process were of analytical reagent grade and were used without further purification.

### 2.2. Instrumentations

The initial pH ($pH_0$) of the dye solution adjusted using a pH meter (SP-701, Suntex, Taiwan) with $H_2SO_4$ or NaOH solutions. X-ray diffraction (XRD) analysis was performed using a Diano-8536 diffractometer equipped with a CuK$\alpha$ radiation source. During analyses, samples were scanned from 20° to 80° at a rate of 0.4° $min^{-1}$. The samples were performed using a superconducting quantum interference device magnetometer (MPMS-XL7, Quantum Design, USA) that was used to determine the magnetic properties of the catalyst. Fluorescence spectroscopy facilitates the complete spectral characterization

of a catalyst material. In this study, fluorescence spectra were obtained using a luminescence spectrophotometer (F-4500, Hitachi, Japan) with a xenon lamp as the excitation source. The emission spectra were plotted on the x-axis, and the excitation spectra were plotted parallel to the y-axis. The widths of all slits in both the excitation and emission monochromators were 10 nm. In this investigation, fluorescence spectra comprised 60 excitation and 60 emission spectra from 200 to 800 nm and provided discrete values of the fluorescence intensity at 3,600 excitation/emission wavelength pairs. Spectral subtraction was performed to remove the blank spectra for pure water. UV-Vis absorption spectra of the solid samples were obtained using a spectrophotometer (U-2900, Hitachi, Japan). The cyclic voltammetry (CV) curves were recorded and were carried out with an electrochemical analyzer (CHI 6081D, CH Instrument, USA) and a three-electrode cell with platinum wire and Ag/AgCl (in a saturated KCl solution) as the counter and reference electrode, respectively. The working electrode was a glassy carbon electrode, and the samples were run at a scan rate of 100 mV s$^{-1}$ with potential cycling between –0.2 and 1.2 V for each analysis. The electrolyte solution was $H_2SO_4$ (0.5 M). The specific surface areas of the composite catalysts were determined from their physical adsorption of nitrogen at 77 K by using a Brunauer–Emmett–Teller (BET) model and a BET surface area analyzer (ASAP 2000, Micromeritics Co., USA). The morphology of the catalyst was carried out on an environmental scanning electron microscopy (ESEM) system equipped with an energy-dispersive X-ray spectrometer (EDS) (Quanta 200 FEG, FEI Company, Czech Republic). These studies yielded information on the distribution of $Fe_3O_4$–CB on the catalyst surface.

### 2.3. Synthesis of iron oxide–carbon black nanoparticle

Magnetic $Fe_3O_4$ particles were prepared through the chemical co-precipitation of $FeCl_3 \bullet 6H_2O$ and $FeCl_2 \bullet 4H_2O$ in alkaline aqueous solutions. The reaction mixture precipitates were thoroughly stirred and added dropwise $NH_4OH$ 30 min and until the pH attained exceeded 9.0 at room temperature. The reaction mixtures further were heated at 353 K for 4 h. The precipitates subjected to washed using deionized water and freeze-dried for further use in experiment. The resulted in the formation of black particles that showed a strong magnetic response. The chemical co-precipitation reaction can be expressed as follows:

$$Fe^{2+} + 2Fe^{3+} + 8OH^- \rightarrow Fe_3O_4 + 4H_2O \qquad (7)$$
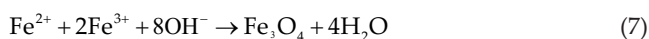
A magnetically responsive $Fe_3O_4$–CB composite catalyst was synthesized using a wet-chemistry approach. In briefly, 100 mg of a Degussa FW200 CB was refluxed within 16 N $HNO_3$ solution, then filtered, washed with deionized water and dried at 333 K in an oven for 6 h. Followed by 5 wt% $Fe_3O_4$ nanoparticle dispersed in the CB matrix using hydroxypropyl cellulose as steric dispersant. After the coating, the mixture was ultrasonicated for 30 min and stirred for 2 h till complete hominization of mixture. The resulting powder was further processed in such way that it formed tablets shaped using acetic acid as a binder. The tablets were further heated at 573 K, and these tablets were calcinated at 573 K in a nitrogen stream for 6 h to burn out the binder.

Followed by the tablets was crushed, sieved with sizes range of 0.25–0.15 mm and directly use for entire experiment without purification. Deionized water was used throughout the experiments for solution preparation. In PS oxidation, MB was used as the target compound.

### 2.4. Degradation experiment

A degradation experimental setup was consisted of a 500-mL cylindrical vessel containing 250 mL of the 15 mg L$^{-1}$ MB dye solution. All of the experiments were conducted at room temperature (298 K). A mechanical stirrer was used to maintain the uniformity of a suspension. When the PS and $Fe_3O_4$–CB powders were added to the solution, the mechanical stirrer was turned on. At different time intervals, 2 mL of the solution was sampled, and its absorbance was measured at 664 nm by using a UV spectrophotometer (Spectroquant Vega 400, Merck, Germany). The decolorization rate ($\eta\%$) was calculated using the formula $\eta\% = (C_0 – C) / C_0 \times 100$, where $C_0$ and $C$ are the absorbance of the sample at times 0 and $t$, respectively. Each decolorization test was run in triplicate, and the average experimental outcomes were used for the results.

## 3. Results and discussion

### 3.1. Decolorization of methylene blue under different conditions

Fig. 1(A) shows the concentrations vs. time curve. The curve comprised decrease in concentrations observed for CB, $Fe_3O_4$–CB, PS, and the $Fe_3O_4$–CB/PS system against time. When only $Fe_3O_4$–CB was used in the effluent, no noticeable removals of MB were observed, indicating the in-effect decolorization of MB under the conditions considered. As shown in Fig. 1(A), it was found that the MB decolorization efficiencies increased to 80%, whereas addition of 0.03 g L$^{-1}$ PS, 0.1 g L$^{-1}$ $Fe_3O_4$–CB, initial pH value of 3.0 at 298 K in $SO_4^{-\bullet}$-based AOPs. Under $Fe_3O_4$–CB/PS process, the preferential degradation was related to the $Fe_3O_4$–CB enhanced aqueous–PS decomposition, thereby generating $SO_4^{-\bullet}$ with a redox potential of 2.6 V and the increase in the mass transfer enhanced the degradation of MB [15–19]. Meanwhile, $S_2O_8^{2-}$ at the $Fe_3O_4$–CB surface could be activated through electron transfer to produce a $SO_4^{-\bullet}$ corresponding to a higher conversion yield, indicating that the use of the combination of $S_2O_8^{2-}$ and $Fe_3O_4$–CB for activated oxidation had a synergistic effect on the decolorization of MB. Nguyen et al. proposed $Fe_3O_4$ magnetic NPs can effectively activate $S_2O_8^{2-}$ to produce $SO_4^{-\bullet}$, which are a powerful oxidant with promising applications to degrade organic contaminants, this may be due to the presence of octahedral sites through the electron transferring to Fe(II) in the $Fe_3O_4$ structure enhancing the production rate of $SO_4^{-\bullet}$ [22]. Furthermore, as the MB PS oxidation reaction proceeded, the degradation kinetics of MB PS oxidation over a $Fe_3O_4$–CB catalyst could be explained by mass-transfer-controlled pseudo-first-order kinetics, as shown by the linear plot of $\ln(C/C_0)$ vs. the reaction time $t$ and the rate constants ($k_{obs}$) of $1.4 \times 10^{-2}$ and $3.6 \times 10^{-2}$ min$^{-1}$ for the PS and $Fe_3O_4$–CB/PS processes, respectively. The increase in the decolorization rate of MB for $Fe_3O_4$–CB/PS processes might be attributable to the increase in the adsorption of MB on $Fe_3O_4$–CB, which in turn increased the extent of surface complexation with MB [35].

When adsorbate in solution is mixed with the catalyst, there occurs transport of the dye into the pores of particles from the solution through the interface between the solution and the catalyst [36]. Also, the adsorption mechanism is mainly followed by ion exchange via releasing exchangeable protons in the interlayer surfaces and also interaction with dye molecules via hydrogen bonding and hydrophobic–hydrophobic mechanisms [28]. However, particle size of a catalyst played a very important role in the catalytic ability of dye. Therefore, further investigation on adsorption mechanism and particle size effect of $Fe_3O_4$–CB/PS processes is to be explored.

Fig. 1(B) depicts the effect of the PS concentration on MB decomposition. The decolorization rate of MB increased sharply with an increase in the PS concentration from 0.01 to 0.12 g $L^{-1}$. Results indicated that approximately 84% MB decolorization was obtained under a PS concentration of 0.12 g $L^{-1}$ and a $Fe_3O_4$–CB dose of 0.1 g $L^{-1}$. A higher PS concentration increased the degradation of MB. It is reasonable that a sufficient amount of PS can produce adequate $SO_4^{-•}$ for increasing the activation activity of $Fe_3O_4$–CB, thereby enhancing the degradation of MB. Moreover, the decomposition of MB in the $Fe_3O_4$–CB/PS system increased with the amount of $SO_4^{-•}$ because of an increase in the direct electron transfer between the constituents of the $Fe^{III}/Fe^{II}$ redox pair conditions [33]. Moreover, the $Fe^{II}$ ion in $Fe_3O_4$ makes this a very efficient catalyst for the degradation of MB and also allows it to be easily separated from the reaction medium using an external magnetic field [35]. Consequently, performing PS oxidation at high PS concentrations increases the production of $SO_4^{-•}$ and provides a strong driving force for the oxidation. The PS oxidation process could also be explained by the synergistic effect of $Fe_3O_4$–CB materials and $SO_4^{-•}$. However, after reaction for 18 min, the decolorization efficiency became slow subsequently as that for the concentration range of 0.03 to 0.12 g $L^{-1}$, which indicated that the activated decomposition of $S_2O_8^{2-}$ by $Fe_3O_4$–CB was rapid as a large number of $SO_4^{-•}$ were generated transiently once Fe(II) contacted with $S_2O_8^{2-}$. Treatment under milder dosage of PS can be a cost-effective condition for dye-contaminated wastewater. Therefore, the optimum amount of PS is found to be 0.03 g $L^{-1}$ for the degradation of MB in this study.

Fig. 2(A) shows the effect of $Fe_3O_4$–CB on the efficiency of MB removal in the $Fe_3O_4$–CB/PS process as a function of time. It was illustrated that the degradation capacity of MB increased sharply with an increase in $Fe_3O_4$–CB from 0.1 to 1.6 g $L^{-1}$. Specifically, Fig. 2(A) shows that when $Fe_3O_4$–CB was used as an activator for effectively degrading MB, a maximum conversion rate of 85% was achieved at a $Fe_3O_4$–CB dose of 1.0 g $L^{-1}$. This observation can be attributed to a sufficient quantity of Fe(II) serving as an electron donor. The PS anions of Fe(II) can be catalytically decomposed to $SO_4^{-•}$ [34]. However, the increase in the degradation rate of MB was negligible when the $Fe_3O_4$–CB dose was further increased to 2.4 g $L^{-1}$. This might be attributable to the formation of a surface precursor between $Fe_3O_4$–CB and MB in a rate-limiting step prior to electron transfer from MB to the active metal center of $Fe_3O_4$–CB, leading to MB depletion [15]. A further increase in the reaction time had little effect on the decolorization rate; this was due to an excess amount of $Fe_3O_4$–CB reducing the consumption of PS. In addition, the produced Fe(II) could scavenge $SO_4^{-•}$ according to Eq. (8), which would account for the decrease in the degradation rate of MB when $Fe_3O_4$–CB/PS was used. This observation is consistent with previously reported results [32]. Therefore, an optimum amount of $Fe_3O_4$–CB is found to be 0.1 g $L^{-1}$ was applied for experiments thereafter.

$$Fe^{2+} + SO_4^{-•} \rightarrow SO_4^{2-} + Fe^{3+} \tag{8}$$

Fig. 2(B) shows plots of the effect of the initial pH on the decolorization of MB in the $Fe_3O_4$–CB/PS system. It can be demonstrated that the effect of pH on MB reduction was strong near $pH_0$ 3.0 and 6.0 after a 3-min reaction at the fast stage, whereas the removal of MB was suppressed at $pH_0$ 9.0. The degradation of MB decreased above $pH_0$ 9.0, most likely because of the precipitation of $Fe^{III}$, which corresponds to the use of $Fe_3O_4$–CB as the catalyst. Moreover, in the $Fe_3O_4$–CB process, the difference in color removal at different $pH_0$ values suggests that the reaction rate of MB in the PS catalytic oxidation system was a pH-dependent process when the generated $SO_4^{-•}$ reacted with $H_2O$ or $OH^-$ to produce hydroxyl
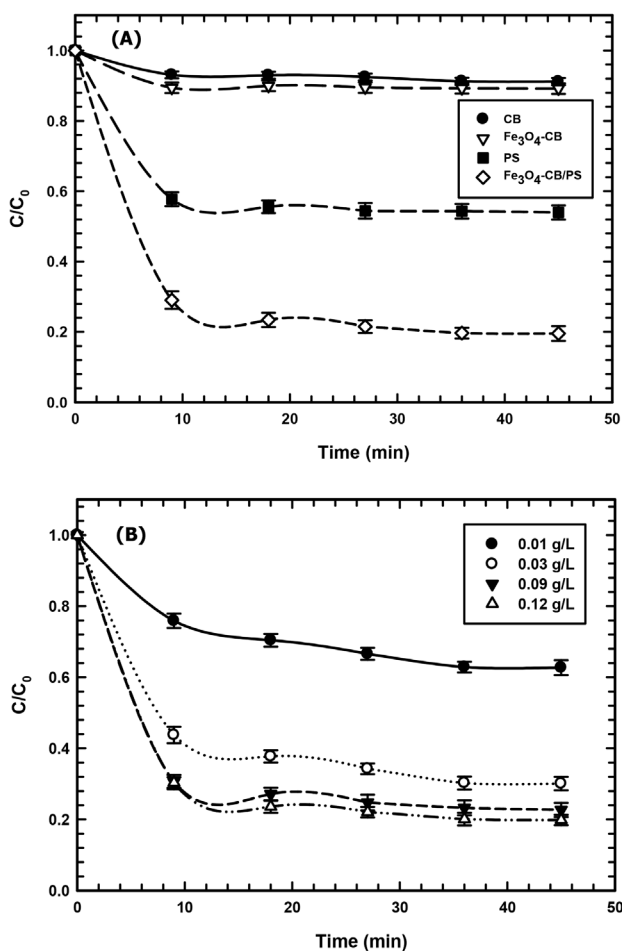


Fig. 1. (A) Plots of the decrease in MB concentration ($C/C_0$) vs. time for different processes with 0.03 g $L^{-1}$ $Na_2S_2O_8$, 0.1 g $L^{-1}$ CB, and 0.1 g $L^{-1}$ $Fe_3O_4$–CB addition. (B) Effect of PS concentration on MB degradation with 0.1 g $L^{-1}$ $Fe_3O_4$–CB addition. Experimental conditions: reaction volume = 250 mL, T = 298 K, $pH_0$ = 3.0, MB = 15 mg $L^{-1}$.

radical species that reduce the solution pH. In addition, acidic conditions are conductive to the dissolution of iron powder because they produce more Fe(II), and therefore, more sulfate radicals can be catalytically formed by Fe(II) through the activation of PS [33]. However, excessive Fe(II) can act as a scavenger of sulfate radicals through electron transfer reactions, thereby reducing the reaction efficiency. These observations indicated that the $Fe_3O_4$–CB concentration should be controlled to minimize the adverse effects of $Fe_3O_4$–CB on $SO_4^{-\bullet}$ production. Under alkaline conditions, more hydroxyl radicals, which are a major reactive oxygen species, were generated from $SO_4^{-\bullet}$ can be explained by the following equation:

$$SO_4^{-\bullet} + OH^- \rightarrow SO_4^{2-} + \bullet OH \tag{9}$$
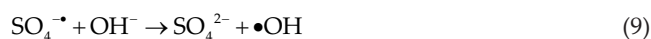
These findings clearly illustrated that the oxidation potential of the $\bullet OH$ may decrease with an increase in pH. Ghaedi et al. indicated this was due to the extinction of the positive hydrogen ions, thereby promoting activities of electrostatic repulsion between the negative charges of both

dye and the catalyst surface [30]. In addition, at a high pH, the scavenging reaction between the $SO_4^{-\bullet}$ and the $\bullet OH$ is enhanced, as follows:

$$SO_4^{-\bullet} + \bullet OH \rightarrow SO_4^{2-} + H^+ + 0.5O_2 \tag{10}$$
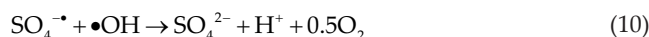
The preceding equations show that the $Fe_3O_4$–CB/PS process can be successfully used for an initial pH in the range of 3.0–9.0. The decolorization rate of MB was heavily dependent on the pH. Therefore, the optimum pH is found to be 3.0 for the degradation of MB in this study. However, further investigation on the role of pH of zero charge and acidic dissociation constant of catalytic process is to be explored.

### 3.2. Characterization of methylene blue under different effects of $Fe_3O_4$/CB

Fig. 3(A) shows XRD patterns of fresh and used catalysts, and it shows that the catalyst changed during exposure to the catalytic environment. Furthermore, it can be seen that the XRD analysis confirmed the existence of the $Fe_3O_4$–CB state in the catalyst. The experimental results showed that the XRD patterns of freshly prepared $Fe_3O_4$–CB and used $Fe_3O_4$–CB after the $Fe_3O_4$–CB/PS processes are similar. The strong XRD peaks (Fig. 3(A)-a) indicate the well-crystallized structure of $Fe_3O_4$ NPs. The dominant $Fe_3O_4$ diffraction peaks detected at 2θ values of approximately 30.1°, 35.5°, 37.2°, 43.2°, 53.6°, 57.0°, 62.7°, and 74.2° are related to the (220), (311), (222), (400), (422), (511), (440), and (533) planes, respectively. Therefore, the diffraction peaks of NPs closely matched those of $Fe_3O_4$ crystals with a cubic structure within the CB, confirming the high crystallinity of the samples. This result agrees closely with that of Yan et al. [23]. The XRD results indicated that $Fe_3O_4$ active sites ($\equiv Fe^{2+}/\equiv Fe^{3+}$) were formed on the $Fe_3O_4$–CB catalyst [37]. Therefore, MB was likely to have been adsorbed on the surface of the catalyst before undergoing a catalytic reaction at the $Fe_3O_4$ active sites. On the basis of XRD patterns, the crystal size of the particles can be evaluated using the following Debye-Scherrer equation:

$$D = K\lambda / (\beta \cos\theta) \tag{11}$$

where $K$ is the Scherrer factor (0.89); $\lambda$ is the X-ray wavelength (0.15418 nm); $\beta$ is the peak full width at half maximum (FWHM); and θ is the Bragg diffraction angle. From the most intense peak (311), the average size of the particles was calculated to be 26.4 nm, which is higher than the reported value for $Fe_3O_4$ (8.9 nm) [38].

Fig. 3(B) shows the magnetic hysteresis loops of fresh and used $Fe_3O_4$–CB samples with a magnetic field cycle between −10 and +10 kOe at 300 K. Both the fresh and used $Fe_3O_4$–CB were magnetic at room temperature, and the M–H hysteresis curves passed the original spot, revealing the super paramagnetic nature of magnetite $Fe_3O_4$–CB materials. The saturation magnetization (Ms) of the fresh and used samples was 31 and 28 emu $g^{-1}$, respectively. This result implies that after the reaction there were no remarkable changes in the magnetic properties of $Fe_3O_4$–CB showed an excellent magnetic response to a magnetic field. Moreover, the observed Ms of $Fe_3O_4$–CB (31 emu $g^{-1}$) is similar to previously reported value (35 emu $g^{-1}$) [39]. Moreover, the advantages of
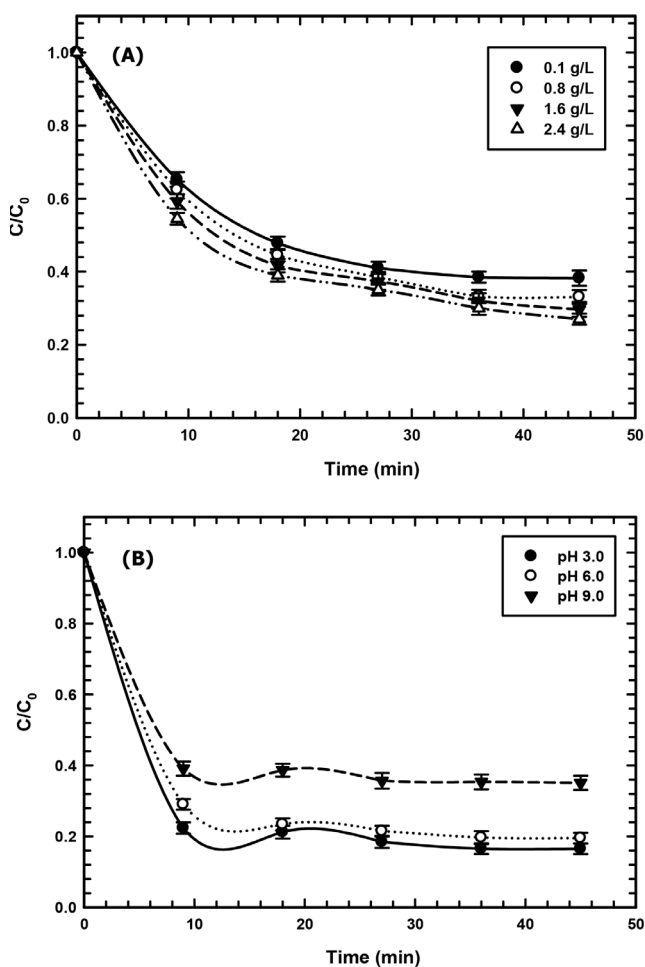


Fig. 2. (A) Effect of $Fe_3O_4$–CB addition and (B) initial pH on MB degradation with 0.1 g $L^{-1}$ $Fe_3O_4$–CB addition. Experimental conditions: reaction volume = 250 mL, T = 298 K, MB = 15 mg $L^{-1}$, $pH_0$ = 3.0, and $Na_2S_2O_8$ = 0.03 g $L^{-1}$.
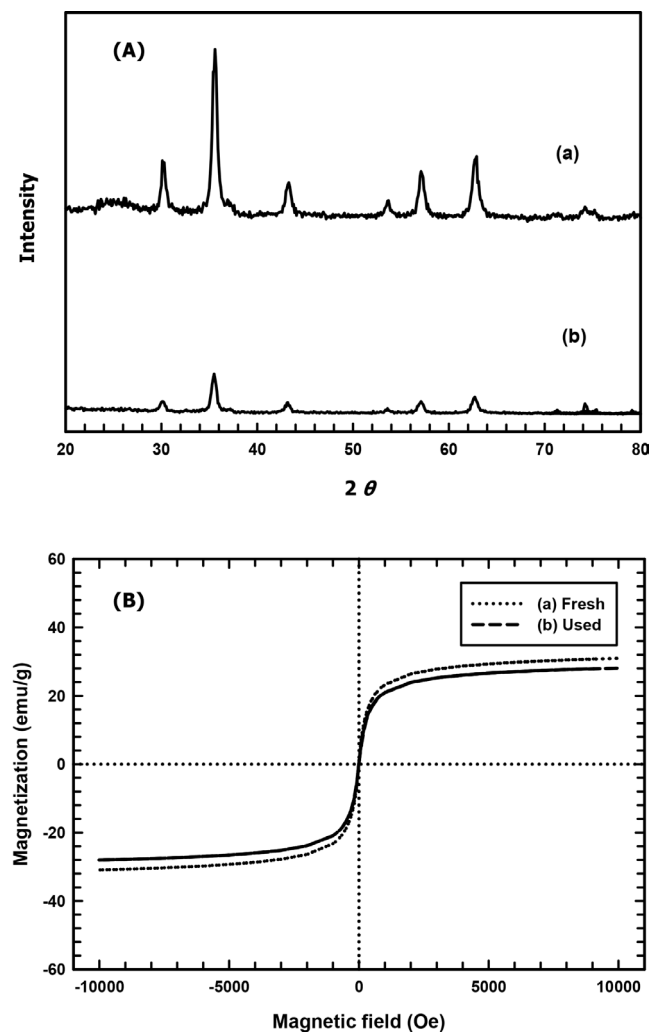
Fig. 3. (A) XRD pattern and (B) magnetic hysteresis loops of the $Fe_3O_4$–CB particle catalyst used in the MB degradation reaction: (a) before and (b) after the catalytic test.





Fig. 4. (A) Fluorescence spectra and (B) UV-Vis absorption spectra of the $Fe_3O_4$–CB particle catalyst in the MB degradation reaction: (a) before and (b) after the catalytic test.

$Fe_3O_4$–CB, which make them valuable for the environment, are having easily separated using external magnet and recyclability of the materials.

In the next step, to further elucidate the reactive properties of the catalyst, excitation plot positions obtained from the fluorescence spectrometer were used for generating effective data for characterizing the properties of the catalyst. Fig. 4(A)-a displays the fluorescence spectra for a fresh $Fe_3O_4$–CB catalyst; two significant excitation peaks at 280, 340, 380, and 470 nm are observed. The $Fe_3O_4$–CB particle showed an increase in its emission wavelength to 380 nm because of the effective transfer of electrons from the excited state to the conduction band of the $Fe_3O_4$–CB particle. This result is similar to that reported by Alveroğlu et al., who observed that the magnetite nanoparticle showed peaks at wavelengths of 380 and 405 nm in the emission spectrum [40]. The fluorescence spectra of the $Fe_3O_4$–CB catalyst after the activity test are shown in Fig. 4(A)-b; large excitation peaks are observed at 280 and 340 nm. These excitation peaks of the catalyst can be described as a metal-enhanced fluorescence effect, in which
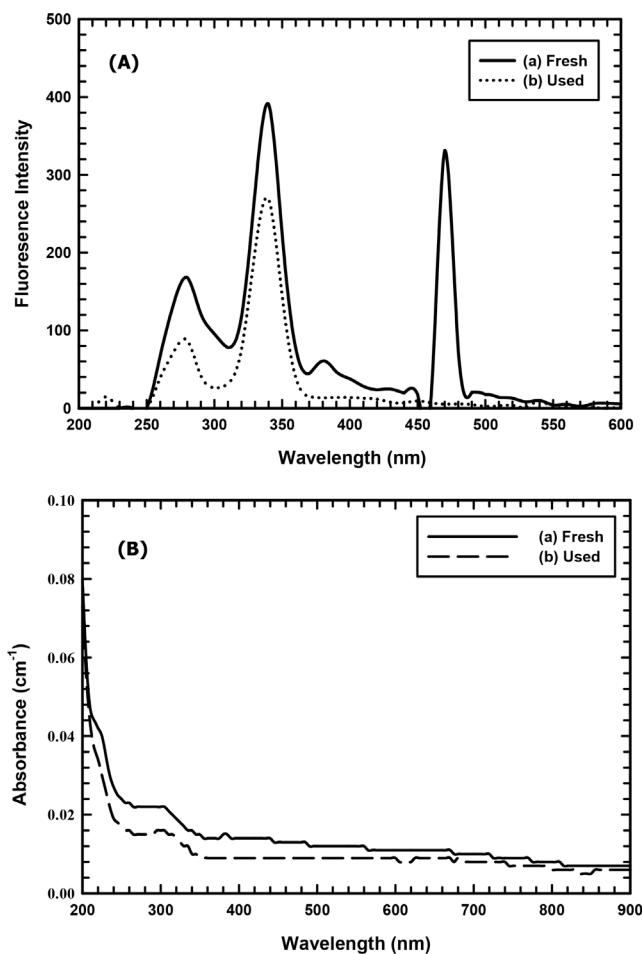
the iron clusters at $Fe_3O_4$–CB catalyst surface sites show fluorescence during the reaction. Moreover, the changes in the observed excitation plots may be due to the presence of surface functional groups and surface energy traps that become emissive on stabilization, following surface passivation after the activity test [41].

To further identify the chemical properties of the $Fe_3O_4$–CB catalyst, Fig. 4(B) presents UV-Vis absorption spectra, which provide more information on the states of iron species in these catalysts. Optical properties associated with such iron particles are observed at 300 nm. Generally, the UV-Vis absorption spectra of a catalyst are related to its molecular and electronic structure. In addition, the measured absorption performance of fresh $Fe_3O_4$–CB is stronger than the exhausted reaction of the $Fe_3O_4$–CB catalyst, which is due to the photon absorption corresponding to Fe particles. However, further investigation on the functional group and acidity and basicity group of catalytic process will be explored in the future.

Fig. 5 shows the electrochemical behavior of the freshly prepared and used $Fe_3O_4$–CB catalysts. The CV plot reveals that the freshly prepared $Fe_3O_4$–CB catalyst showed a higher reversible redox ability and oxidation current density than the used $Fe_3O_4$–CB catalyst, with the well-marked state

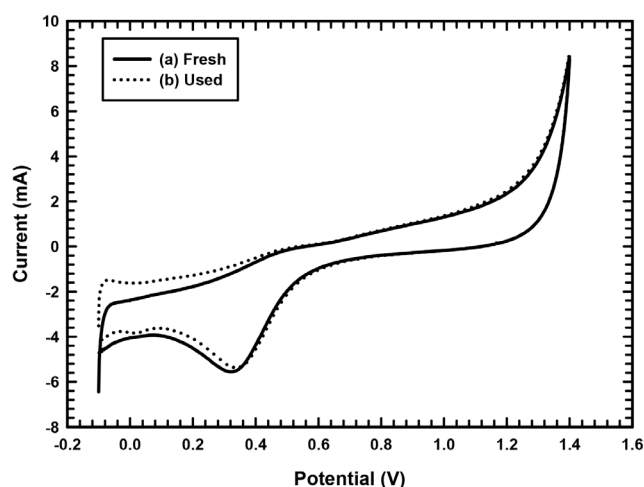Fig. 5. CV profiles of the $Fe_3O_4$–CB particle catalyst in a 0.5 M $Na_2SO_4$ electrolyte solution in the degradation of MB at a scan rate of 100 mV s$^{-1}$: (a) before and (b) after the catalytic test.

being at 0.55 and 0.61 V for the freshly prepared and used $Fe_3O_4$–CB catalysts, respectively. This reversible redox ability of the fresh catalyst could explain the high activity of the catalysts. By contrast, the used $Fe_3O_4$–CB catalyst produced negligible oxidation–reduction currents in this potential window. Lambrou et al. demonstrated that $Fe_3O_4$ has the most active phase in the catalytic reaction because this compound strongly promotes oxygen storage [42]. This finding suggests that $Fe_3O_4$–CB has the ability to promote the activation of PS during MB oxidation. Furthermore, the generation of $Fe_3O_4$ species was evidenced by reduction peaks near 0.6 V [43,44]. Therefore, MB is believed to be adsorbed onto the surface of the catalyst before the oxidation–reduction cycle reaction commences at the $Fe_3O_4$ active sites ($\equiv Fe^{2+}/\equiv Fe^{3+}$).

The adsorptive and catalytic behavior of a catalyst is strongly influenced by the capacity and texture of its exterior surface. Fig. 6 summarizes the test catalysts properties, including $N_2$ adsorption–desorption isotherms and specific surface area, determined by BET analysis. The specific surface area of the fresh $Fe_3O_4$–CB catalyst was 1,965 m$^2$ g$^{-1}$. For the used $Fe_3O_4$–CB catalyst, the surface area showed a slight decrease (1,895 m$^2$ g$^{-1}$). This test showed that the catalysts were associated with a larger lattice surface of iron or CB and that higher loadings caused metal sintering, possibly reducing catalytic activity. Reaction conditions clearly play a crucial role in activating the generated surface, and an increase in the surface area may not be the main factor promoting catalytic activity. The good catalytic performance of the composites could be attributed to synergy between the functions of the CB support and the $Fe_3O_4$ NPs embedded in the carrier [45].

Fig. 7 presents ESEM–EDS images of the surface morphology changes of the $Fe_3O_4$–CB particle catalyst. These data provide crucial information about the surface structure of the catalyst during the MB oxidation reaction. ESEM observations of the particles indicated that the $Fe_3O_4$–CB catalyst formed small $Fe_3O_4$ spherical particles dispersed in the CB matrix sizes of 50–100 nm. In addition, these results confirmed that the dispersion of the catalyst increased the
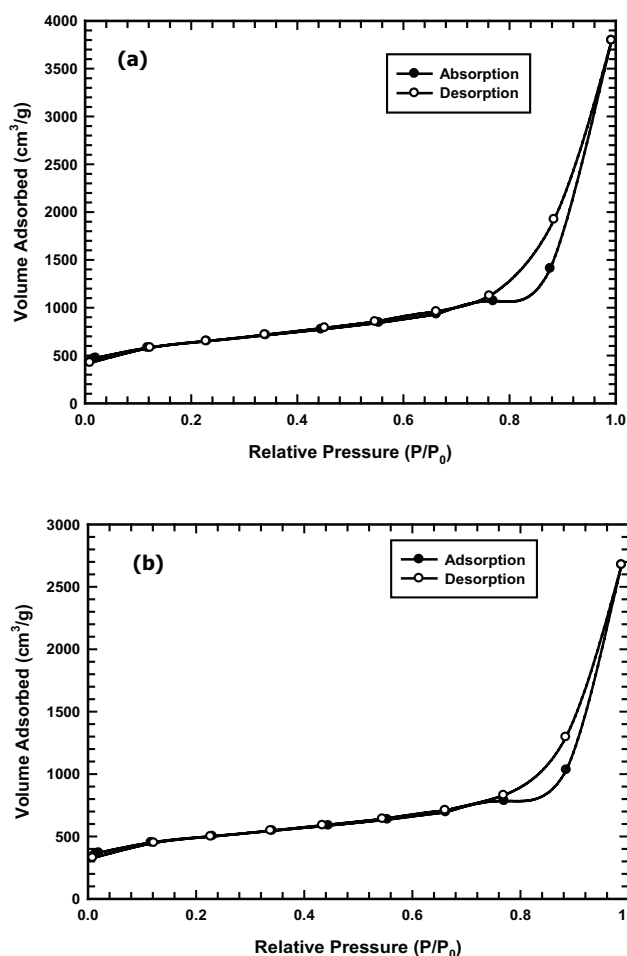


Fig. 6. $N_2$ adsorption–desorption isotherms of the $Fe_3O_4$–CB particle catalyst used in the MB degradation reaction: (a) before and (b) after the catalytic test.

efficiency of MB catalysis. Fig. 7(a) also shows that the catalyst surface is more crystalline than that observed in Fig. 7(b). The small crystal phases may explain the high activity of the catalysts, which have a nanoscale particle size, which show high dispersion. These structural properties are useful for the removal of MB from water. Specifically, the particles agglomerated when the catalyst surface aged or was poisoned because of plugging, implying a change in the porosity of the particles (Fig. 7(b)). The EDS result elucidates that iron, carbon, and oxygen species were the major elements of the coating in the catalyst structure. Moreover, the elemental composition analysis of the test catalyst surfaces revealed that $Fe_3O_4$–CB was eluted from the catalyst, possibly exposing the active sites ($\equiv Fe^{2+}/\equiv Fe^{3+}$) of the catalyst NPs. The performance of the $Fe_3O_4$–CB catalyst was degraded mainly because of iron corrosion, which led to the agglomeration of NPs on the surface of $Fe_3O_4$.

## 4. Conclusions

The potential of the decolorized process for the removal of MB indicated that the optimum conditions over a reaction time of 24 min and for an optimal initial
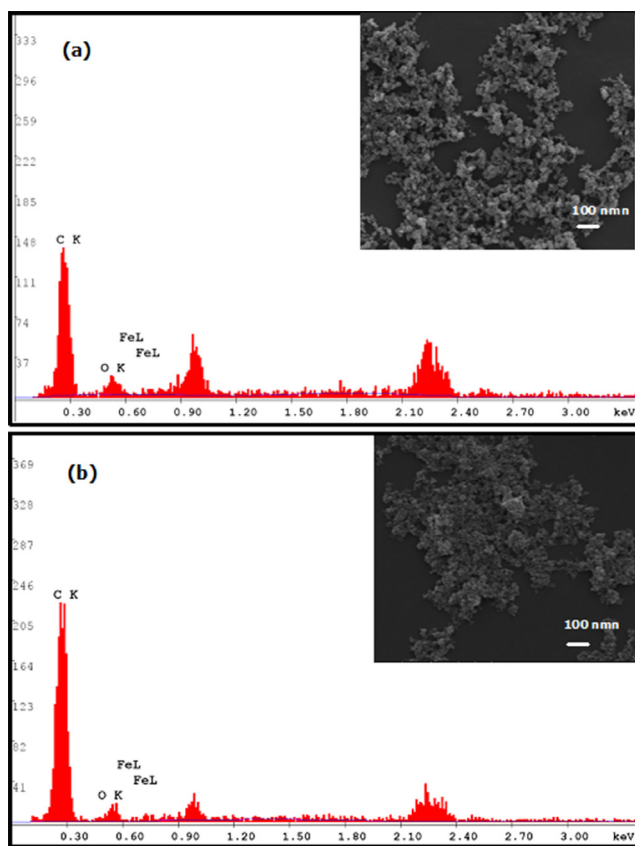
Fig. 7. ESEM–EDS photographs of the $Fe_3O_4$–CB particle catalyst used in the MB degradation reaction: (a) before and (b) after the catalytic test.

## References

[1] S.T. Ong, P.S. Keng, W.N. Lee, S.T. Ha, Y.T. Hung, Dye waste treatment, Water, 3 (2011) 157–176.

[2] M. Pu, Y. Ma, J. Wa, Y. Wang, M. Huang, Y. Chen, Fe/S doped granular activated carbon as a highly active heterogeneous persulfate catalyst toward the degradation of Orange G and diethyl phthalate, J. Colloid Interface Sci., 418 (2014) 330–337.

[3] C.M. Hung, C.W. Chen, Y.J. Jhuang, C.D. Dong, $Fe_3O_4$ magnetic nanoparticles: characterization and performance exemplified by the degradation of methylene blue in the presence of persulfate, J. Adv. Oxid. Technol., 19 (2016) 43–51.

[4] M. Jamshidi, H.Z. Khafri, A. Asfaram, A. Goudarzi, Response surface methodology approach for optimization of adsorption of Janus Green B from aqueous solution onto $ZnO/Zn(OH)_2$-NP-AC: kinetic and isotherm study, Spectrochim. Acta, Part A, 152 (2016) 233–240.

[5] M. Ghaedi, K. Dashtiana, A.M. Ghaedi, S. Hajati, A. Goudarzi, E. Alipanahpour, Highly efficient simultaneous ultrasonic assisted adsorption of brilliant green and eosin B onto ZnS nanoparticles loaded activated carbon: artificial neural network modeling and central composite design optimization, Spectrochim. Acta, Part A, 153 (2016) 257–267.

[6] A. Asfaram, M. Ghaedi, A. Goudarzi, M. Rajabi, Response surface methodology approach for optimization of simultaneous dye and metal ion ultrasound-assisted adsorption onto Mn doped $Fe_3O_4$-NPs loaded on AC: kinetic and isothermal studies, Dalton Trans., 44 (2015) 14707–14723.

[7] E.A. Dil, M. Ghaedi, A.M. Ghaedi, A. Asfaram, A. Goudarzi, S. Hajati, M. Soylak, S. Agarwal, V.K. Gupta, Modeling of quaternary dyes adsorption onto ZnO–NR–AC artificial neural network: analysis by derivative spectrophotometry, J. Ind. Eng. Chem., 34 (2016) 186–197.

[8] Y. Hou, J. Qu, X. Zhao, P. Lei, D. Wan, C. Huang, Electro-photocatalytic degradation of acid orange II using a novel $TiO_2$/ACF photoanode, Sci. Total Environ., 407 (2009) 2431–2439.

[9] A. Asfaram, M. Ghaedi, S. Hajati, A. Goudarzi, Ternary dye adsorption onto $MnO_2$ nanoparticle-loaded activated carbon: derivative spectrophotometry and modeling, RSC Adv., 5 (2015) 72300–72320.

[10] M. Roosta, M. Ghaedi, F. Yousefi, Optimization of the combined ultrasonic assisted/adsorption method for the removal of malachite green by zinc sulfide nanoparticles loaded on activated carbon: experimental design, RSC Adv., 5 (2015) 100129–100141.

[11] M. Dastkhoon, M. Ghaedi, A. Asfaram, A. Goudarzi, S.M. Langroodi, I. Tyagi, S. Agarwal, V.K. Gupta, Ultrasound assisted adsorption of malachite green dye onto ZnS:Cu-NP-AC: equilibrium isotherms and kinetic studies-response surface optimization, Sep. Purif. Technol., 156 (2015) 780–788.

[12] F. Duarte, F.J. Maldonado-Hódar, L.M. Madeira, Influence of the particle size of activated carbons on their performance as Fe supports for developing Fenton-like catalysts, Ind. Eng. Chem. Res., 51 (2012) 9218–9226.

[13] X. Wang, L. Wang, J. Li, J. Qiu, C. Cai, H. Zhang, Degradation of Acid Orange 7 by persulfate activated with zero valent iron in the presence of ultrasonic irradiation, Sep. Purif. Technol., 122 (2014) 41–46.

[14] A.A. Bazrafshan, S. Hajati, M. Ghaedi, Synthesis of regenerable $Zn(OH)_2$ nanoparticle-loaded activated carbon for the ultrasound-assisted removal of malachite green: optimization, isotherm and kinetics, RSC Adv., 5 (2015) 79119–79128.

[15] A. Yang, C. Huang, B. Wei, Z. Zhang, Facile decolorization of methylene blue with flower-like manganese wads, Water Sci. Technol., 69 (2014) 1094–1100.

pH of 3.0 at an MB concentration of 15 mg $L^{-1}$, a PS concentration of 0.03 g $L^{-1}$, and a $Fe_3O_4$–CB dose of 1.0 g $L^{-1}$. The valence of $Fe_3O_4$ changed from +2 to +3 when the $SO_4^{-\bullet}$ directed electron transfer between the $Fe_3O_4$–CB composites interface. The reaction kinetics with respect to MB was assigned a pseudo-first-order rate. Overall, PS plays a great synergistic role on $Fe_3O_4$–CB, and the $SO_4^{-\bullet}$-based AOPs reaction activity of $Fe_3O_4$–CB is closely related to MB degradation function. Moreover, the loss of activity of the $Fe_3O_4$–CB particle catalyst was attributed to over-oxidation of the catalyst surface or inhibition of the surface by reaction intermediates. Specifically, the $Fe_3O_4$–CB particle catalyst was crucial because it was involved in the PS oxidation of MB, unlike $Fe_3O_4$–CB, which appeared to provide only active sites ($\equiv Fe^{2+}/\equiv Fe^{3+}$) for the reaction during the catalytic run. This behavior was attributed to synergistic structural and functional effect of the combined $Fe_3O_4$ NPs and CB. Therefore, these results proved that high treatment efficiency can be achieved for the degradation of dye aqueous solutions and help achieve environmental sustainability by $Fe_3O_4$–CB/PS process. The data and methodology presented in this work might be useful for designing the heterogeneous catalyst for the treatment of actual effluents. However, further investigation on stability and reusability of $Fe_3O_4$–CB composites and economic analysis is to be explored.

[16] A. Tsitonaki, B. Petri, M. Crimi, H. Mosbaek, R.L. Siegrist, P.L. Bjerg, In situ chemical oxidation of contaminated soil and groundwater using persulfate: a review, Crit. Rev. Env. Sci. Technol., 40 (2010) 55–91.

[17] X.R. Xu, S. Li, Q. Hao, J.L. Liu, Y.Y. Yu, H.B. Li, Activation of persulfate and its environmental application, Inter. J. Environ. Bioenergy, 1 (2012) 60–81.

[18] C.H. Yen, K.F. Chen, C.M. Kao, S.H. Liang, T.Y. Chen, Application of persulfate to remediate petroleum hydrocarbon-contaminated soil: feasibility and comparison with common oxidants, J. Hazard. Mater., 186 (2011) 2097–2012.

[19] S.H. Do, Y.J. Kwon, S.H. Kong, Effect of metal oxides on the reactivity of persulfate/Fe(II) in the remediation of diesel-contaminated soil and sand, J. Hazard. Mater., 182 (2010) 933–936.

[20] A. Ghauch, A.M. Tuqan, N. Kibbi, S. Geryes, Methylene blue discoloration by heated persulfate in aqueous solution, Chem. Eng. J., 213 (2012) 259–271.

[21] L. Zhu, Z. Ai, W. Ho, L. Zhang, Core–shell $Fe–Fe_2O_3$ nanostructures as effective persulfate activator for degradation of methyl orange, Sep. Purif. Technol., 108 (2013) 159–165.

[22] T.D. Nguyen, N.H. Phan, M.H. Do, K.T. Ngo, Magnetic $Fe_2MO_4$ (M:Fe, Mn) activated carbons: fabrication, characterization and heterogeneous Fenton oxidation of methyl orange, J. Hazard. Mater., 185 (2011) 653–661.

[23] J. Yan, M. Lei, L. Zhu, M.N. Anjum, J. Zou, H. Tang, Degradation of sulfamonomethoxine with $Fe_3O_4$ magnetic nanoparticles as heterogeneous activator of persulfate, J. Hazard. Mater., 186 (2011) 1398–1404.

[24] X.R. Xu, X.Z. Li, Degradation of azo dye Orange G in aqueous solutions by persulfate with ferrous ion, Sep. Purif. Technol., 72 (2010) 105–111.

[25] S.Y. Yang, X. Yang, X.T. Shao, R. Niu, L.L. Wang, Activated carbon catalyzed persulfate oxidation of azo dye acid orange 7 at ambient temperature, J. Hazard. Mater., 186 (2011) 659–666.

[26] X. Yu, S. Ye, Recent advances in activity and durability enhancement of Pt/C catalytic cathode in PEMFC: Part II: degradation mechanism and durability enhancement of carbon supported platinum catalyst, J. Power Sources, 172 (2007) 145–154.

[27] H. Mazaheri, M. Ghaedi, S. Hajati, K. Dashtian, M.K. Purkait, Simultaneous removal of methylene blue and $Pb^{2+}$ ions using ruthenium nanoparticle-loaded activated carbon: response surface methodology, RSC Adv., 5 (2015) 83427–83435.

[28] F.N. Azad, M. Ghaedi, K. Dashtian, S. Hajati, A. Goudarzic, M. Jamshidi, Enhanced simultaneous removal of malachite green and safranin O by ZnO nanorod-loaded activated carbon: modeling, optimization and adsorption isotherms, New J. Chem., 39 (2015) 7998–8005.

[29] A. Asfaram, M. Ghaedi, S. Hajati, A. Goudarzi, A.A. Bazrafshan, Simultaneous ultrasound-assisted ternary adsorption of dyes onto copper-doped zinc sulfide nanoparticles loaded on activated carbon: optimization by response surface methodology, Spectrochim. Acta, Part A, 145 (2015) 203–212.

[30] M. Ghaedi, M.R. Rahimi, A.M. Ghaedi, I. Tyagi, S. Agarwal, V.K. Gupta, Application of least squares support vector regression and linear multiple regression for modeling removal of methyl

[31] Y.C. Lee, S.L. Lo, J. Kuo, C.P. Huang, Promoted degradation of perfluorooctanic acid by persulfate when adding activated carbon, J. Hazard. Mater., 261 (2013) 463–469.

[32] C. Tan, N. Gao, W. Chu, C. Li, M.R. Temoleton, Degradation of diuron by persulfate activated with ferrous ion, Sep. Purif. Technol., 95 (2012) 44–48.

[33] S.C.N. Tang, I.M.C. Lo, Magnetic nanoparticles: essential factors for sustainable environmental applications, Water Res., 47 (2013) 2613–2632.

[34] J. Anotai, N. Masomboon, C.L. Chuang, M.C. Lu, Persulfate oxidation for the aniline degradation in aqueous systems, Water Sci. Technol., 63 (2011) 1434–1440.

[35] L. Zhou, Y. Shao, J. Liu, Z. Ye, H. Zhang, J. Ma, Y. Jia, W. Gao, Y. Li, Preparation and characterization of magnetic porous carbon microspheres for removal of methylene blue by a heterogeneous Fenton reaction, ACS Appl. Mater. Interfaces, 6 (2014) 7275–7285.

[36] Y. Sağ, Y. Aktay, Mass transfer and equilibrium studies for the sorption of chromium ions onto chitin, Process Biochem., 36 (2000) 157–173.

[37] B. Kakavandi, A. Takdastan, N. Jaafarzadeh, M. Azizi, A. Mirzaei, A. Azari, Application of $Fe_3O_4$@C catalyzing heterogeneous UV-Fenton system for tetracycline removal with a focus on optimization by a response surface method, J. Photochem. Photobiol., A, 314 (2016) 178–188.

[38] H. Meng, Z. Zhang, F. Zhao, T. Qiu, J. Yang, Orthogonal optimization design for preparation of $Fe_3O_4$ nanoparticles via chemical coprecipitation, Appl. Surf. Sci., 280 (2013) 679–685.

[39] T.S. Atabaev, H.K. Kim, Y.H. Hwang, Fabrication of bifunctional core-shell $Fe_3O_4$ particles coated with ultrathin phosphor layer, Nanoscale Res. Lett., 8 (2013) 357–363.

[40] E. Alveroğlu, H. Sözeri, A. Baykal, U. Kurtan, M. Şenel, Fluorescence and magnetic properties of hydrogels containing $Fe_3O_4$ nanoparticles, J. Mol. Struct., 1037 (2013) 361–366.

[41] X. He, Y. Liu, H. Li, H. Huang, J. Liu, Z. Kang, S.T. Lee, Photoluminescent $Fe_3O_4$/carbon nanocomposite with magnetic property, J. Colloid Interface Sci., 356 (2011) 107–110.

[42] P.S. Lambrou, A.M. Efstathiou, The effects of Fe on the oxygen storage and release properties of model $Pd–Rh/CeO_2–Al_2O_3$ three-way catalyst, J. Catal., 240 (2006) 182–193.

[43] C. Karunakaran, J. Jayabharathi, R. Sathishkumar, Interaction of fluorescent sensor with superparamagnetic iron oxide nanoparticles, Spectrochim. Acta, Part A, 110 (2013) 151–156.

[44] F. Wu, R. Huang, D. Mu, B. Wu, S. Chen, New synthesis of a foamlike $Fe_3O_4$/C composite via a self-expanding process and its electrochemical performance as anode material for lithium-ion batteries, ACS Appl. Mater. Interfaces, 6 (2014) 19254–19264.

[45] N.A. Zubir, C. Yacou, J. Motuzas, X. Zhang, J.C.D. Costa, Structural and functional investigation of graphene oxide–$Fe_3O_4$ nanocomposites for the heterogeneous Fenton-like reaction, Sci. Rep., 4 (2014) 1–8.